Applied Thermal Engineering 31 (2011) 2716–2725

Contents lists available at ScienceDirect

Applied Thermal Engineering

journal homepage: www.elsevier.com/locate/apthermeng

Effect of brine flow rate on the performance of a spiral-jacketed thermal storage tank used for SDHW systems: A computational fluid dynamics study

Seung Man Baek [a], Jin Hyun Nam [b], Hiki Hong [c], Charn-Jung Kim [a,*]

[a] School of Mechanical and Aerospace Engineering, Seoul National University, San 56-1, Shilim-dong, Gwanak-gu, Seoul 151-742, Republic of Korea
[b] School of Automotive, Industrial, and Mechanical Engineering, Daegu University, Gyungsan 712-714, Republic of Korea
[c] School of Mechanical System Engineering, Kyung Hee University, Yongin 449-701, Republic of Korea

ARTICLE INFO

Article history:
Received 15 July 2010
Accepted 27 April 2011
Available online 13 May 2011

Keywords:
Solar thermal energy
Solar domestic hot water system
Thermal storage tank
Mantle heat exchanger
Spiral brine path
Computational fluid dynamics

ABSTRACT

This study numerically investigates the effect of the brine flow rate on the thermal performance of a spiral-jacketed thermal storage tank (TST) installed in a solar domestic hot water (SDHW) system. The spiral-jacketed TST is a TST with a mantle heat exchanger, consisting of a vertical, cylindrical water tank for energy storage and a spiral brine flow path attached to the tank wall for heat transfer. A computational fluid dynamics (CFD) model was constructed based on the actual geometry of a spiral-jacketed TST. In addition, the boundary conditions were defined by considering solar radiation and ambient temperature data that were measured during experimental operation of the SDHW system. The numerical results demonstrated that an increase in the brine flow rate enhances the thermal efficiency of the TST due to higher heat transfer coefficients in the spiral path, and also leads to reduced thermal stratification in the TST. On the other hand, a lower brine flow rate increased the heat transfer rate at the inlet of the spiral path near the top of the TST, which resulted in enhanced thermal stratification. The optimal range for the rate of brine flow rate is discussed with respect to the thermal efficiency of the TST and the required pumping power for brine circulation in the spiral flow path.

1. Introduction

Solar energy is the fundamental source of all types of energy currently used by humans, including fossil fuels, hydraulic power, and wind power. Solar energy is almost unlimited in its supply, has minimal environmental impact, and is available free of charge. In fact, solar thermal energy has long been utilized to reduce the energy requirements for heating in both domestic and industrial settings [1,2]. In addition, photovoltaic cells are currently the focus of extensive research efforts to develop alternative methods of electrical energy production by direct conversion of solar energy. Thus, solar energy is expected to be an important source of renewable energy in the future.

A typical example of solar energy utilization is solar domestic hot water (SDHW) systems that collect and store solar thermal energy in the form of hot water for domestic use. An SDHW system consists of roof-mounted solar panels for solar energy collection, single or multiple thermal storage tanks (TSTs) for hot water storage, a liquid pump for the circulation of brine (heat transfer fluid) between the solar panels and the TSTs, and a liquid-to-liquid heat exchanger for energy transfer from brine to water in the TSTs. In general, an SDHW is also equipped with auxiliary electric heaters for additional water heating and an automatic controller for the operation of the entire system.

Conventional SDHW systems primarily use immersed coil heat exchangers [3] or external shell and tube heat exchangers [4,5] for the transfer of energy from the brine to the water in the TST. There are also other types of heat exchangers available for solar heating applications, such as flat-plate and tube-in-tube heat exchangers [6]. Regarding alternative heat exchangers for SDHW systems, several researchers have recently studied the performance of TSTs equipped with mantle heat exchangers [7–15]. The mantle heat exchanger is, in fact, an annular flow path for brine attached to a TST through which hot brine is circulated; this allows for the transfer of heat to the water in the TST. This simple and cost-effective concept is an important advantage of mantle heat exchangers over conventional heat exchangers [8].

The performance of a TST in an SDHW system can be evaluated by determining the ratio of the thermal energy stored in the TST to the total solar radiation incident on the collector panels during a given period. However, this performance estimate, which is based on the average water temperature, may not properly account for

* Corresponding author. Tel.: +82 2 880 1662; fax: +82 2 883 0179.
E-mail address: kimcj@snu.ac.kr (C.-J. Kim).

1359-4311/$ – see front matter © 2011 Elsevier Ltd. All rights reserved.
doi:10.1016/j.applthermaleng.2011.04.043

effectiveness with respect to the thermal stratification within the TST. For example, a TST with more thermal stratification can provide a larger amount of hot water at a fixed average temperature compared to a TST with less thermal stratification. In that case, an exergy analysis may be a better choice to evaluate the performance of a TST [16–18]. In addition, the quantity of electrical power consumed by liquid pumps should also be included in the exergy analysis for a comprehensive assessment of SDHW systems.

In this study, computational fluid dynamics (CFD) simulations were performed to investigate the effect of the brine flow rate on the performance of a spiral-jacketed TST. A spiral-jacketed TST is composed of a vertical cylindrical tank for thermal energy storage and a spiral flow path attached to the tank wall for heat transfer (a mantle heat exchanger). The performance of an SDHW system with a spiral-jacketed TST was the subject of previous experimental studies by Reindl et al. [19]. In addition, Nam et al. [20] developed a CFD model of the spiral-jacketed TST and verified its reliability by comparing the simulation results to the measured performance.

Thus, based on the CFD model established by Nam et al. [20], this study quantitatively investigates the effect of the brine flow rate on the acquired thermal energy and thermal stratification in the spiral-jacketed TST, as well as the heat transfer characteristics of the spiral flow path. The optimal flow rate for brine circulation is also discussed by considering both the thermal performance of the TST and the required pumping power for the system.

2. Theory and calculations

2.1. SDHW system

Fig. 1 shows a schematic diagram of the SDHW system with a spiral-jacketed TST that was considered in this study. As illustrated in Fig. 1, the spiral-jacketed TST is a mantle-type TST in which a spiral flow path for the brine is attached to the tank wall for heat transfer. The SDHW system shown in Fig. 1 is the same system as was used in the experimental study by Reindl et al. [19]. The authors of that study demonstrated that an SDHW system with a spiral-jacketed TST could greatly reduce system complexity as well as installation and maintenance costs compared to conventional systems with an external heat exchanger; however, the thermal performance was slightly reduced by about 6–11%.

In Fig. 1, the SDHW system consists of two circuits: one circuit for brine that circulates between the solar collector panels and the mantle heat exchanger attached to the TST, and the other circuit for city water that is stored and heated inside the TST, and then supplied as domestic hot water. The brine circuit consists of solar collector panels, a liquid pump, a spiral mantle heat exchanger, and an automatic control unit. The brine is heated in the collector panels by absorbing solar energy, after which it is pumped toward the TST. Subsequently, the hot brine flows through the spiral heat exchanger and transfers thermal energy to the water in the TST, and it then returns to the solar collector panels. The automatic controller monitors the temperature at the inlet and outlet of the solar collector panel and controls the brine flow with the liquid pump.

The water circuit consists of a vertical cylindrical TST, an auxiliary heater, a liquid pump, and a power converter. The cold water is supplied to the TST through the inlet near the bottom of the tank. While it is stored inside the TST, the city water is heated by acquiring energy from the hot brine that circulates through the spiral mantle heat exchanger. When it is needed, the hot water is discharged from the TST through the outlet near the top of the TST. The auxiliary heater and the power converter are operated as needed to increase the temperature of the hot water supply to an adequate level for household use. Detailed specifications of the SDHW system are provided in Table 1 [19].

2.2. CFD model

The CFD model of the spiral-jacketed TST is shown in Fig. 2; the grid structure, the locations of the brine inlet and outlet, and the dimensions of the TST and the spiral flow path are presented. The capacity of the vertical cylindrical TST was about 400 ℓ, with a diameter, D, of 608 mm and a height, H, of 1410 mm. Liquid water stored in the TST was assumed to be at rest, with a uniform temperature distribution (17.8 °C) at the beginning of the charging process.

As shown in Fig. 2, hot brine from the collector panels enters through the inlet near the top of the TST, travels along the spiral flow path, and then exits through the outlet near the bottom. The spiral flow path has a rectangular cross-section (100 mm width by 15 mm height) and wraps nine times around the TST. As the hot

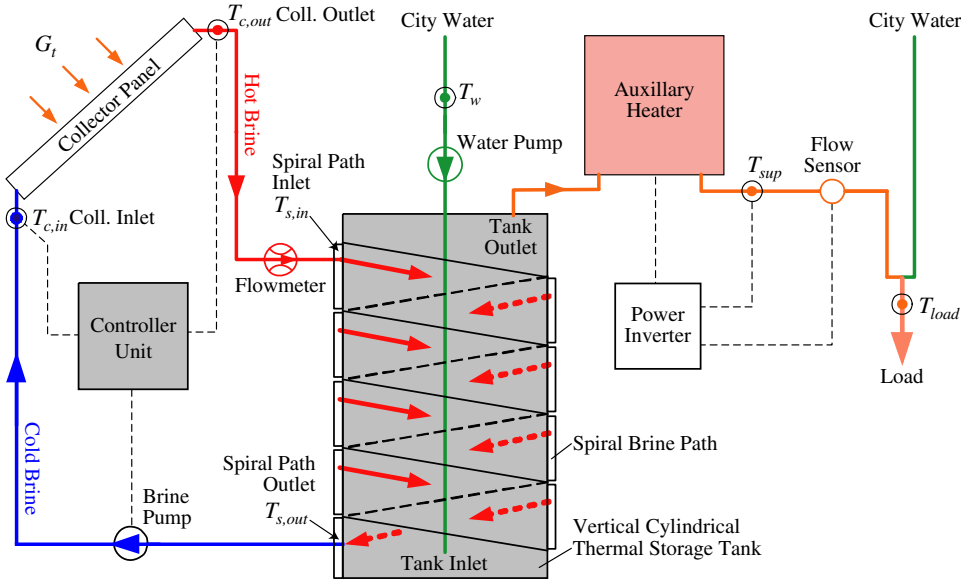

Fig. 1. Schematic diagram of an SDHW system equipped with a spiral-jacketed TST.

Table 1
Detailed specifications for the SDHW system considered in this study, adopted from Reindl et al. [19].

Solar collector panel	Type	Flat-plate
	Dimension	1179 mm × 2228 mm
	Number of units	4 (serial connection)
	Area	10 m^2 (4 × 2.5 m^2)
	Slope	40° (fixed)
Thermal storage tank	Type	Vertical cylinder
	Dimension	297 mm (D) × 1410 mm (H)
	Capacity	400 ℓ
	Material	Sheet steel (enamel-coated)
Heat exchanger	Type	Mantle (spiral-jacketed)
	Channel dimension	100 mm (W) × 15 mm (H)
	Pitch	120 mm
Brine pump	Type	Centrifugal
	Capacity	60 ℓ/min (at 4 m pump head)
	Rated power	80 W
Controller module	Type	Temperature control (on/off)
Auxiliary heater	Type	Instant electric heater
	Capacity	13.2 kW
Pipe	Diameter	20 mm
	Material	Copper or steel
Insulation	Material	Polyurethane (100 mm)
Heat transfer fluid	Material	Water/propylene glycol mixture

brine flows through the spiral flow path, thermal energy is transferred from the brine to the water in the TST via the side wall. The heat transfer from the tank wall causes slow natural convection of liquid water inside the TST, characterized by an upward motion of the liquid water near the heated wall and a downward motion near the center.

A 40%(wt) mixture of propylene glycol (PG) and water was used as the brine in the spiral path to prevent freezing in cold weather conditions [19]. The physical properties of the water and brine considered in this study are summarized in Table 2. The wall of the TST was made of a 3.2 mm-thick sheet of steel and was coated with corrosion-resistant enamel (0.25 mm thick) on both sides. An adiabatic condition was imposed on the top, bottom, and circumference of the calculation domain due to the polyurethane foam insulation (100 mm thick).

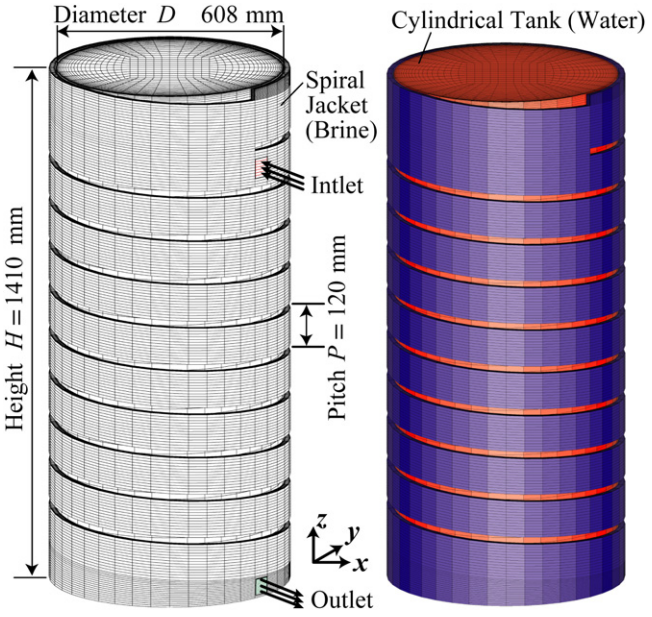

Fig. 2. Configuration and numerical grids used for the spiral-jacketed TST.

Table 2
Physical Properties for fluids in the spiral-jacketed TST.

Fluid	Properties	Values
Water [a] (inside the TST)	Density, ρ_w	998 kg m^{-3}
	Viscosity, μ_w	0.000889 Pa s
	Specific heat, c_{pw}	4182 J kg^{-1} K^{-1}
	Conductivity, k_w	0.62 W m^{-1} K^{-1}
Brine PG/water mixture (40 wt%) (inside the spiral path)	Density, ρ_b	1040 kg m^{-3}
	Viscosity, μ_b	0.00211 Pa s
	Specific heat, c_{pb}	4185 J kg^{-1} K^{-1}
	Conductivity, k_b	0.416 W m^{-1} K^{-1}

[a] These properties are the representative values at 25 °C. In actual CFD simulations, temperature-dependent properties were used except the density of water.

The computational grid was generated separately for three regions: the cylindrical TST for water storage, the spiral flow path for brine circulation, and the enamel-coated tank wall. The grid for the TST was constructed based on a structured 'O-grid' topology to obtain a better resolution for the non-axisymmetric flow structures. In addition, a smaller grid size of about 1 mm was used near the tank wall to capture the large gradient of temperature and velocity distribution in that region. The grid for the spiral flow path was designed with a rectangular cross-section of 13 cells in the width direction and 10 cells in the height direction. The grid for the tank wall was created using three layers of cells for the steel plate with enamel coating. Then, the total number of finite volume cells was 166,000: 88,200 cells were used for the TST, 67,000 cells were used for the spiral path, and 10,800 cells were used for the tank wall.

2.3. Governing equations

The fluid flow and heat transfer in the spiral-jacketed TST are governed by the conservation of mass, momentum, and energy. For an incompressible fluid, the conservation of mass, or the continuity equation, is written as

$$\frac{\partial u_j}{\partial x_j} = 0, \tag{1}$$

where x_j (j = 1,2,3) is the direction in the Cartesian coordinate system, and u_j is the velocity component in that direction.

The conservation of momentum, or the Navier–Stokes equation is written as

$$\rho\left(\frac{\partial u_i}{\partial t} + u_j\frac{\partial u_i}{\partial x_j}\right) = -\frac{\partial p}{\partial x_i} + \mu\frac{\partial^2 u_i}{\partial x_j \partial x_j} - \rho g_i \beta\left(T - T_{\mathrm{ref}}\right), \tag{2}$$

where ρ is the density, p is the pressure, μ is the dynamic viscosity, g_i is the gravitational acceleration, β is the volume expansion coefficient, and T is the temperature which is a variable in time, $T(t)$. In Eq. (2), the Boussinesq approximation is used to account for the density variation with respect to temperature.

As shown in Eq. (2), this study assumes that laminar flow is prevalent in the liquid water flow inside the TST. The Rayleigh number was estimated to be on the order of 10^{12} during the charging process of the TST. According to Qureshi and Gebhart [21], the transition toward turbulent flow occurs at about 10^{13} if the liquid water is heated by a vertical wall with a constant heat flux condition. For example, using the laminar flow equations, Papanicolaou and Belessiotis [22] successfully calculated the transient natural convection of liquid water in a cylindrical enclosure up to a Rayleigh number of 10^{13}.

Note that the laminar flow equation of Eq. (2) was also used, without the Boussinesq term, to calculate the brine flow in the spiral path of the TST. At some high flow rates considered in this

study, the brine flow in the spiral jacket corresponded to turbulent flow regime. However, it was found that turbulent flow calculation had only minimal effects on the overall simulation results (the acquired heat and the overall heat transfer coefficient), compared to laminar flow calculation. Thus, laminar flow calculation was employed for the brine flow in the spiral jacket irrespective of the brine flow rate, focusing more on low flow rate conditions.

The equation for the conservation of energy is written as

$$\rho c_p\left(\frac{\partial T}{\partial t}+u_j\frac{\partial T}{\partial x_j}\right) = \frac{\partial}{\partial x_j}\left(k\frac{\partial T}{\partial x_j}\right), \quad (3)$$

where c_p is the specific heat at constant pressure and k is the thermal conductivity. Note that Eq. (3) is the standard conduction–convection equation for energy transport and conservation. For solid regions, u_j in Eq. (3) should be zero to reflect a pure conduction process.

2.4. Brine inlet conditions

The thermal efficiency of the spiral-jacketed TST shown in Fig. 2 can be estimated by simulating the charging process with a fixed inlet temperature for the brine. However, the efficiency of the TST can be more accurately evaluated with respect to the SDHW system by employing more realistic conditions for the brine temperature at the inlet of the spiral heat exchanger. Because the brine circuit in the SDHW system forms a closed circulation loop, as shown in Fig. 1, the brine temperature at the inlet of the spiral heat exchanger is directly influenced by the brine temperature at the outlet. In addition, the thermal energy collected in the solar panels should also be considered to properly track the variation of the brine temperature.

In this study, the brine temperature at the inlet of the spiral flow path was calculated at the beginning of each time step based on the outlet temperature at the previous time step and actual solar radiation data. Fig. 3 shows the solar radiation intensity incident on the collector panels, G_t, and th with the following expressions:

$$G_t(t) = 619.82 + 233.18t - 84.25t^2 + 7.131t^3\left(R^2 = 0.939\right), \quad (4)$$

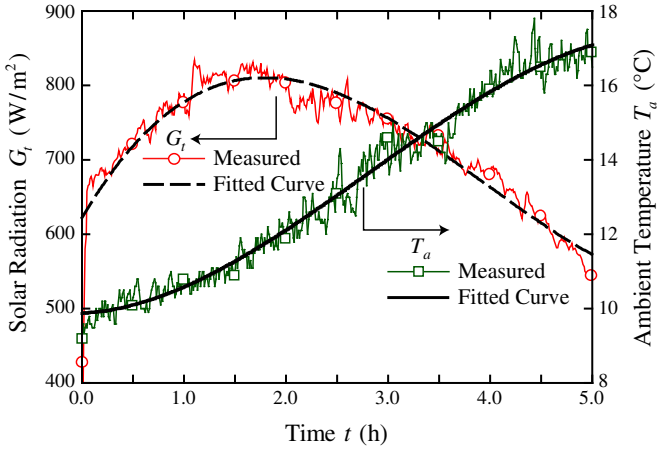

Fig. 3. Solar radiation and ambient temperature conditions measured during an experiment on Nov. 31, 2005.

$$T_a(t) = 9.88 + 0.136t - 0.644t^2 - 0.0767t^3\left(R^2 = 0.989\right), \quad (5)$$

where t is the time in hours, and R^2 is the coefficient of determination.

If heat loss in the pipes is neglected, then the brine temperature at the inlet of the collector panels, $T_{c,\text{in}}$, becomes the same as that at the outlet the spiral flow path, $T_{s,\text{out}}$. Likewise, the brine temperature at the inlet of the spiral flow path, $T_{s,\text{in}}$, becomes the same as the outlet temperature of the collector panels, $T_{c,\text{out}}$. Thus, the temperature difference between the inlet and the outlet of the collector panels, $\Delta T_c \equiv T_{c,\text{out}} - T_{c,\text{in}}$, is similar to the temperature difference between the inlet and the outlet of the spiral heat exchanger, $\Delta T_s \equiv T_{s,\text{in}} - T_{s,\text{out}}$, i.e., $\Delta T_c = \Delta T_s$.

The collection efficiency of the solar panels, η_c, can be expressed as [1]

$$\eta_c = \frac{\dot{m}c_p\Delta T_c}{G_t A_c} = F_R(\tau\alpha) - F_R U_L\frac{T_{c,\text{avg}} - T_a}{G_t}, \quad (6)$$

where $\dot{m}$ is the mass flow rate of the brine, G_t is the incident radiation intensity, A_c is the total collecting area, F_R is the collector heat removal factor, $\tau\alpha$ is the transmittance-absorptance product, U_L is the overall heat loss coefficient, T_a is the ambient temperature, and $T_{c,\text{avg}}$ is the average brine temperature in the collector panels, which is calculated as $T_{c,\text{avg}} = (T_{c,\text{in}} + T_{c,\text{out}})/2$. By rearranging Eq. (6), the inlet-outlet temperature difference for the solar collector panels, ΔT_c, can be written as

$$\Delta T_c = T_{c,\text{out}} - T_{c,\text{in}} = \frac{G_t A_c F_R(\tau\alpha) - F_R U_L A_c\left(T_{c,\text{avg}} - T_a\right)}{\dot{m}c_p}. \quad (7)$$

In Eq. (7), A_c was set to 10 m^2 because four 2.5 m^2 flat-plate collectors were connected in series to absorb solar thermal energy. In addition, two characteristic parameters for the solar collector panels, $F_R(\tau\alpha)$ and $F_R U_L$, were estimated as 0.7321 and 6.1021 W/m^2-K, respectively [1]. To determine ΔT_c, the measured incident radiation intensity, $G_t(t)$, in Eq. (4) and the ambient temperature, $T_a(t)$, in Eq. (5) were substituted into Eq. (7). To examine the effect of the brine flow rate, five different values of $\dot{m}$ (2, 4, 8, 16, and 32 ℓ/min) were considered in this study.

In the calculation, the brine temperature at the inlet of the spiral heat exchanger, $T_{s,\text{in}}$, was determined at the beginning of each time step as follows:

$$T_{s,\text{in}} = \begin{cases} T_0, & t = 0 \\ T_{s,\text{out}}^{\text{old}} + \Delta T_c, & t > 0 \end{cases}. \quad (8)$$

Here, T_0 is the initial temperature of the brine (17.8 °C) at $t = 0$, and $T_{s,out}^{old}$ is the brine temperature at the outlet of the spiral flow path as determined in the previous time step. Eq. (8) uses the equality of $\Delta T_s = \Delta T_c$ that was derived from the assumption of negligible heat loss in the pipes. In addition, the heat capacitances of the liquid pump, collector panels, and various piping components are also neglected in Eq. (8).

The present model was focused on the detailed heat transfer and fluid flow calculation for the spiral-jacketed TST, while the other part of the system, such as the solar collector panels, was approximated by the semi-empirical formula, Eq. (6). In addition, this study considered the radiation intensity and the ambient temperature, Eqs. (4) and (5), which were measured during a day in the fall season. Thus, it should be noted that the present model may have limited capabilities for predicting the overall performance of SDHW systems. For more accurate prediction of the SDHW system performance, the thermal behaviors of the solar collector panels and pipes should be considered in the CFD model using relevant zero-dimensional models, and also the seasonal variation of solar and ambient conditions.

2.5. Numerical procedure

The fluid flow and heat transfer in the spiral-jacketed TST were simulated using the commercial CFD software, STAR-CD (CD-Adapco, Korea), which is based on the finite volume method. The temporal and the spatial discretization of the governing equations were achieved using the first-order implicit Euler method and the second-order monotone advection and reconstruction scheme (MARS), respectively. The velocity-pressure coupling in the transient simulation was solved using the pressure implicit splitting of operators (PISO) algorithm. The spiral-jacketed TST undergoing a 5-h charging process was simulated with a constant time step size of 6 s, which required transient calculations for a total of 3000 time steps. The time step size of 6 s was chosen considering both the accuracy and efficiency of the CFD simulations.

3. Results and discussion

3.1. Model validation

The present numerical calculation is based on the same CFD model for SDHW systems developed previously by the authors [20]. Thus, the validity of the present model was indirectly demonstrated by referring to the results of our previous study. The grid size and time step dependency tests were also performed in the development of the CFD model. The validation test results excerpted from our previous study [20] are shown in Fig. 4, where $E_{t,1h}$ denotes the energy acquired by the spiral-jacketed TST per hour. Note that the brine flow rate was fixed at 24.8 ℓ/min.

Fig. 4 shows that the simulated $E_{t,1h}$ was much higher than the experimentally determined value for the first hour. A smaller value for $E_{t,1h}$ was obtained in the experiment because the brine circulation pump was stopped for about 13.5 min at the beginning of the experiment. During this period, some solar energy accumulated inside the collector panels along with an increase in the collector temperature. This, in turn, resulted in a slightly higher experimental $E_{t,1h}$ compared to the simulated $E_{t,1h}$ in the second hour, as indicated in Fig. 4. The difference in the experimental and the numerical $E_{t,1h}$ for the third and fourth hours without pump interruption was less than 1%.

The total energy acquired by the spiral-jacketed TST during the 5-h charging process, $E_{t,5h}$, could be obtained by summing up hourly $E_{t,1h}$ shown in Fig. 4. The experimental $E_{t,5h}$ was about 52.9 MJ, which corresponds to 40.6% of the total solar radiation energy (about 130.3 MJ) incident on the collector panels. Similarly, the numerical $E_{t,5h}$ from the CFD simulation was about 56.0 MJ (43.0% of total solar radiation). Then, the difference between the experimental and the numerical $E_{t,5h}$ was estimated to be about 5.5% (3.1 MJ/56.0 MJ), with the difference being due primarily to the variation in the experimental conditions. Thus, the reliability of the present CFD model was validated by relatively good agreement between the experimental and numerical performances.

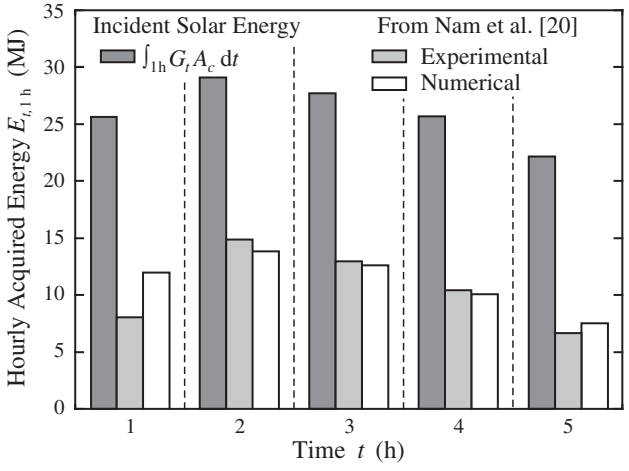

Fig. 4. Thermal performance results for validation of the present numerical model adopted from Nam et al. [20].

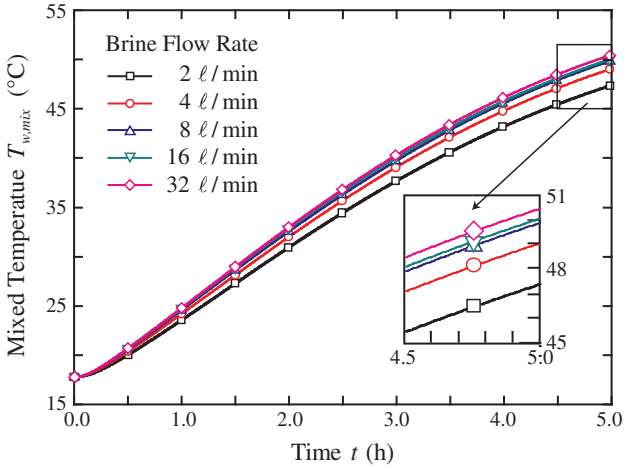

Fig. 5. Evolution of the mixed temperature in the spiral-jacketed TST with variations in the brine flow rate.

3.2. Thermal performance

Fig. 5 shows the temporal evolution of the mixed temperature, $T_{w,mix}$, for the water stored in the spiral-jacketed TST during the 5-h charging process. The mixed temperature was calculated in the CFD simulations as

$$T_{w,\mathrm{mix}} = \frac{\sum_i T_{w,i}\Delta V_i}{\sum_i \Delta V_i}, \tag{9}$$

where $T_{w,i}$ is the temperature of a finite volume cell i corresponding to the cylindrical fluid region, and ΔV_i is the volume of the cell. Fig. 5 clearly indicates that the mixed temperature increases faster with time when the brine flow rate, Q_b, is higher. However, the effect of the brine flow rate on the mixed temperature is less noticeable as the magnitude of Q_b becomes greater than 8 ℓ/min.

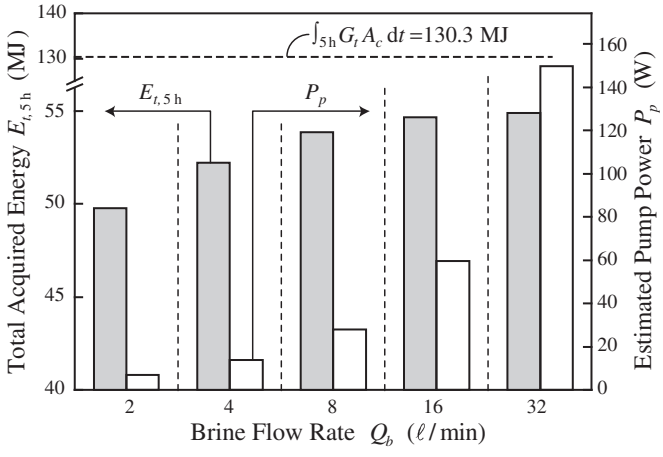

Fig. 6. Overall thermal performance of the spiral-jacketed TST with variations in the brine flow rate.

Table 3
Summary of simulation results for the spiral-jacketed TST operated with different brine flow rates.

Q_b	$T_{w,\mathrm{mix}}$	$\Delta T_{w,5\ \mathrm{h}}$	$E_{t,5\ \mathrm{h}}$	$\Xi_{t,5\ \mathrm{h}}$	η_{th}	P_p	t_{circ}	$\overline{UA}$	$\Xi_{t,5\ \mathrm{h}} - \int_{5\ \mathrm{h}} P_p dt$
2 ℓ/min	47.4 °C	13.1 °C	50.7 MJ	2.46 MJ	38.90%	6.8 W	160 min	116.6 W/K	2.33 MJ
4 ℓ/min	49.1 °C	10.1 °C	52.2 MJ	2.70 MJ	40.02%	13.7 W	121 min	187.9 W/K	2.45 MJ
8 ℓ/min	49.9 °C	7.7 °C	53.8 MJ	2.83 MJ	41.32%	27.8 W	86 min	270.8 W/K	2.33 MJ
16 ℓ/min	50.1 °C	6.6 °C	54.7 MJ	2.86 MJ	41.95%	59.5 W	74 min	337.8 W/K	1.79 MJ
32 ℓ/min	50.5 °C	5.6 °C	54.9 MJ	2.92 MJ	42.11%	149.6 W	63 min	396.9 W/K	0.23 MJ

The mixed temperature is directly related to the energy acquired by the TST, E_t, as expressed by

$$E_t = \rho_w c_{pw} V_t (T_{w,\mathrm{mix}} - T_{w,0}), \tag{10}$$

where V_t is the total volume of the TST (about 400 ℓ). Fig. 6 compares the total thermal energy collected by the solar panels, $\int_{5\mathrm{h}} G_t A_c dt$ = 130.3 MJ, and the total acquired energy of the TST, $E_{t,5\mathrm{h}}$, for different brine flow rates. Fig. 6 also shows that a higher Q_b generally increases the total amount of energy acquired by the TST. In this model, the thermal energy loss through the 10-cm thick polyurethane foam insulator was ignored. A post-simulation analysis showed that this thermal loss was only about 0.5% of $E_{t,5\mathrm{h}}$ for an assumed temperature difference of 30 °C.

A quantitative summary of the performance of the spiral-jacketed TST in the SDHW system is provided in Table 3, in which the thermal performance of the TST, η_{th}, is defined as

$$\eta_{\mathrm{th}} = \frac{E_{t,5\mathrm{h}}}{\int_{5\mathrm{h}} G_t A_c dt} \times 100\%. \tag{11}$$

For the SDHW system shown in Fig. 1, a higher brine flow rate tends to reduce the average temperature of the brine that circulates through the tubes, pumps, and solar collector panels. This reduction in the brine temperature decreases the loss of thermal energy to the surroundings, as modeled in Eqs. (6) and (7). Thus, a higher η_{th} at a higher brine flow rate can be partially attributed to this reduction in heat transfer to the ambient air.

In Table 3, the thermal efficiency, η_{th}, increases only slightly by about 3.21 percentage points (from 38.90% to 42.11%) when the brine flow rate is increased by a factor of 16 from 2 ℓ/min to 32 ℓ/min. Note that the pumping power is also an important factor that affects the performance of an SDHW system. Thus, the pumping power, P_p, was estimated as

$$P_p = \frac{\rho_b g \Delta h Q_b}{\eta_p}, \tag{12}$$

where Δh is the pump head and η_p is the pump efficiency (assumed to be 0.5). The pump head was assumed to be the sum of the static pressure head corresponding to 10 m elevation and the viscous pressure head corresponding to brine flow through straight 20 m pipe of 2 cm diameter. The estimated pumping power is presented in Fig. 6, in which a nonlinear dependence of P_p on Q_b, as indicated in Eq. (12), can be observed. The estimated pump power is relatively small (6.8 W for Q_b = 2 ℓ/min), but it becomes very large, reaching 149.6 W for Q_b = 32 ℓ/min This high power consumption to maintain brine circulation seems to be too large for an SDHW system.

In addition to the energy analysis, an exergy analysis is also frequently conducted to evaluate the performance of a TST in an SDHW system [16–18]. Exergy is defined as the maximum amount of useful work extracted during an ideal process that brings the system into equilibrium with ambient conditions. Thus, the exergy of the TST, Ξ_t, was calculated in the CFD simulations as

$$\Xi_t = \sum_i \rho_w c_{pw} \left[(T_{w,i} - T_{w,0}) - T_{w,0} \ln(T_{w,i}/T_{w,0}) \right] \Delta V_i, \tag{13}$$

where the ambient temperature was assumed to be equal to the initial water temperature, $T_{w,0}$. The exergy in the TST at the end of the charging process, $\Xi_{t,5\mathrm{h}}$, is summarized in Table 3. In addition, the net exergy of the TST, $\Xi_{t,net}$, was calculated by subtracting the total work required to pump the brine for 5 h from $\Xi_{t,5\mathrm{h}}$, such that [16]

$$\Xi_{t,\mathrm{net}} = E_t - \int_{5\mathrm{h}} P_p dt. \tag{14}$$

In Table 3, the net exergy of the TST is highest at the brine flow rate of Q_b = 4 ℓ/min. Based on this result, the optimal range for Q_b was assumed to be around 4 ℓ/min.

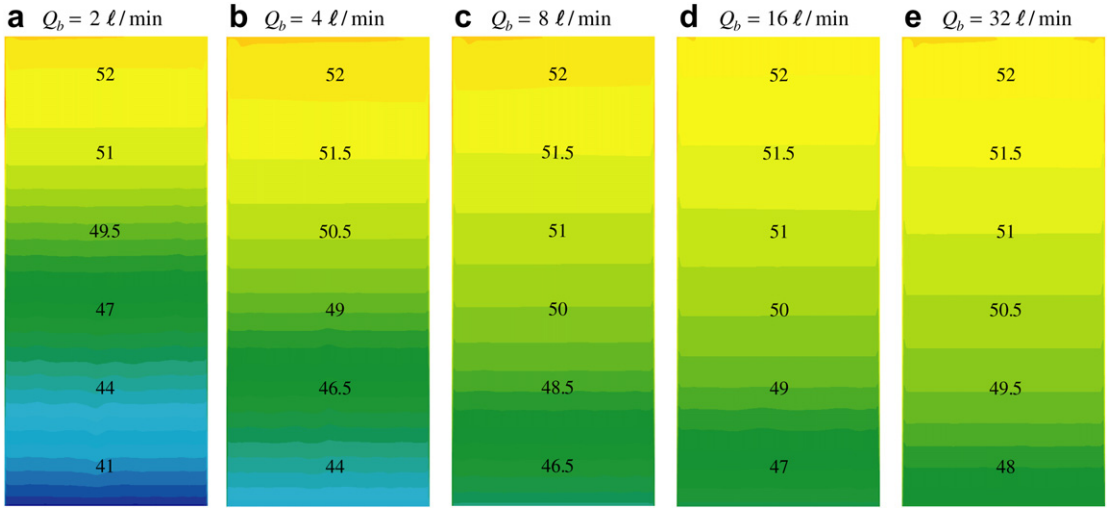

Fig. 7. Final distribution of temperature in the mid-plane of the spiral-jacketed TST at t = 5 h: (a) Q_b = 2 ℓ/min, (b) Q_b = 4 ℓ/min, (c) Q_b = 8 ℓ/min, (d) Q_b = 16 ℓ/min, and (e) Q_b = 32 ℓ/min.

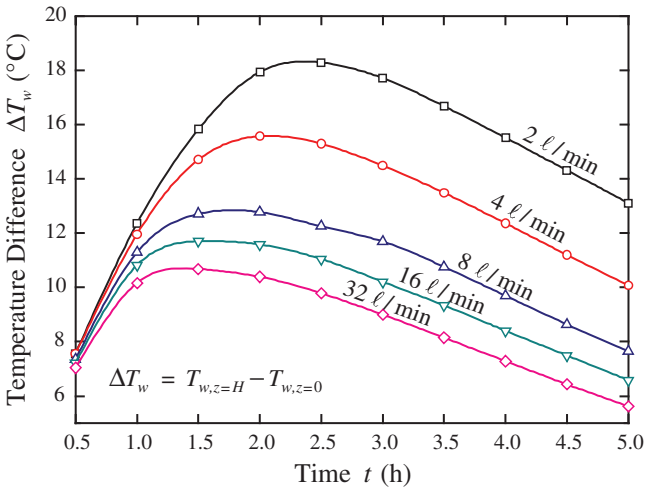

Fig. 8. Temperature difference between the top and the bottom of the spiral-jacketed TST.

3.3. Thermal stratification

The performance of the spiral-jacketed TST was quantitatively evaluated in the previous section by considering the amount of energy and exergy that were stored at the end of the 5-h charging process. In addition to those parameters, the thermal stratification in the TST was also recognized as an important factor for improving the performance of SDHW systems [23]. For an SDHW system with an external heat exchanger, higher thermal stratification lowers the return temperature of water toward the external heat exchanger, which, in turn, reduces the return temperature of the brine toward the solar collector panels. The efficiency of solar collector panels generally increases when the return temperature of the brine is reduced. Thus, extensive research has been conducted to minimize mixing and thus improve thermal stratification in TSTs by using internal baffles or porous structures as well as by optimizing geometry and positions of the inlet and outlet [24–26]. For an SDHW system with a mantle heat exchanger, higher thermal stratification in the TST is also desirable to obtain better performance for the same reason [12,14].

Fig. 7 shows the simulated distribution of hot water temperature in the mid-plane of the TST after the 5-h charging process. The temperature distribution in Fig. 7 clearly indicates that thermal stratification develops in the TST due to natural convection induced by the buoyant motion of the heated water near the tank wall. In Fig. 7, the highest temperature is found at the top of the TST and remains relatively constant around 52 °C regardless of the brine flow rate. In contrast, the lowest temperature observed at the bottom becomes significantly higher as the brine flow rate increases. In Fig. 7, the degree of thermal stratification in the TST tends to decrease at higher Q_b, mainly because the water temperature at the lower part of the TST increases by storing more heat (higher average temperature). Also note that the temperature distribution in the upper one-third region of the TST is insensitive to the brine flow rate.

The temperature difference between the top and the bottom of the TST, ΔT_w, is presented in Fig. 8. The brine flow rate is observed to greatly affect the thermal stratification in the spiral-jacketed TST.

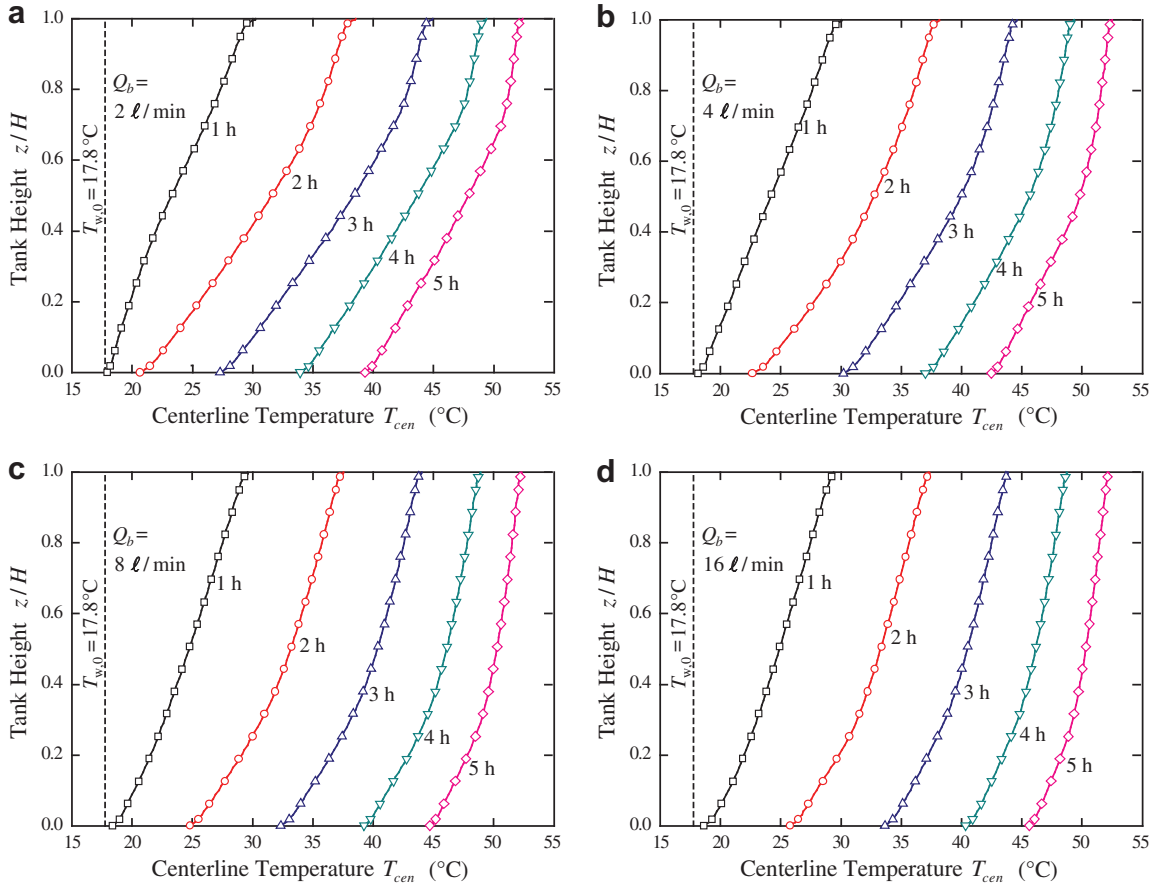

Fig. 9. Temperature distribution along the centerline of the spiral-jacketed TST: (a) Q_b = 2 ℓ/min, (b) Q_b = 4 ℓ/min, (c) Q_b = 8 ℓ/min, and (d) Q_b = 16 ℓ/min.

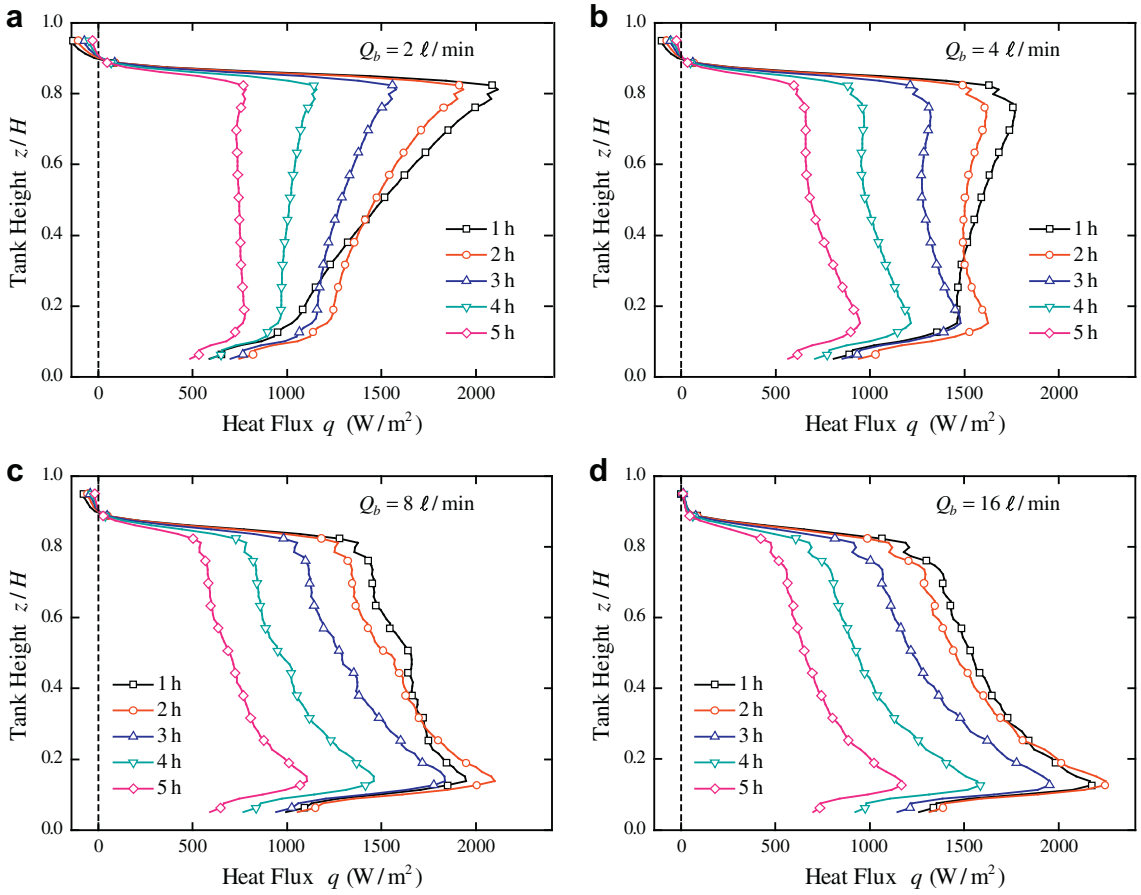

Fig. 10. Heat flux distribution at the heated wall of the spiral-jacketed TST: (a) $Q_b = 2$ ℓ/min, (b) $Q_b = 4$ ℓ/min, (c) $Q_b = 8$ ℓ/min, and (d) $Q_b = 16$ ℓ/min.

For example, ΔT_w at the end of the charging process ($t = 5$ *h*) is relatively large as 13.1 °C for $Q_b = 4$ ℓ/min, but it decreases to 5.6 °C as Q_b increases to 32 ℓ/min. See Table 3 for ΔT_w at $t = 5$ *h* for other brine flow rates. In Fig. 8, a peak in the temperature difference is always observed at around 1–2 h, which is the direct result of the peak in the incident solar radiation, G_t, shown in Fig. 3. However, the time at which the peak ΔT_w occurs is retarded as the brine flow rate decreases, which indicates a slower response of the SDHW system to the incident solar radiation at lower brine flow rates.

Fig. 9 shows the temperature distribution in the z-coordinate along the centerline of the TST. The temperature along the centerline, $T_{w,\mathrm{cen}}$, is considered to be a representative value because the temperature gradient in the horizontal plane of the TST is negligible, as shown in Fig. 7. In addition, the plots for $Q_b = 32$ ℓ/min were omitted in Fig. 9 because they were similar to the plots for $Q_b = 16$ ℓ/min. The initial water temperature in the TST was set to 17.8 °C according to the experimental conditions. Fig. 9 shows that water temperature slowly increases during the 5-h charging process due to the transfer of solar energy from the brine to the water. The temperature increase is most noticeable between $t = 1$ *h* and $t = 3$ *h*, which is the time during which the solar radiation is greatest. In Fig. 9, the effect of the brine flow rate on the temperature at the top of the TST ($z/H = 1$) is almost negligible, whereas the effect on the temperature at the bottom ($z = 0$) is significant. In summary, a higher brine flow rate is found to enhance the thermal performance of the TST by increasing the water temperature in the range of $0 < z/H < 0.7$, while decreasing thermal stratification.

At this moment, it should be noted that only a partial aspect of thermal stratification was discussed in the present study. In general, thermal stratification becomes more important in the situation when the hot water in the TST is actually being used, i.e., hot water is drawn off from the top of the TST while cold water is supplied from the bottom. In this situation, mixing within the water tank should be minimized in order to obtain the maximum thermal efficiency. Thus, a CFD calculation with full consideration of charging/discharging of water can provide more complete assessment of the thermal stratification in the spiral-jacketed TST.

3.4. Heat transfer characteristics

To clarify the effect of the brine flow rate, the heat transfer characteristics for the spiral-jacketed TST were investigated in detail. Fig. 10 shows the temporal evolution of the heat flux distribution at the tank wall for different brine flow rates. In Fig. 10, the plots for $Q_b = 32$ ℓ/min were omitted as before. The heat flux, q, was obtained by averaging the calculated heat flux values around the circumference of the TST. Fig. 10 clearly shows that the distribution of the wall heat flux is strongly influenced by the brine flow rate. For $Q_b = 2$ ℓ/min, the highest wall heat flux is generally observed near $z/H = 0.8$, which is the location of the inlet of the spiral flow path. In contrast, for $Q_b > 8$ ℓ/min, the highest q is always found near $z/H = 0.1$, which is the location of the outlet of the spiral brine path. For $Q_b = 4$ ℓ/min, the wall heat flux exhibits the most uniform distribution with a maximum value at around $z/H = 0.8$ for $t < 1$ h and at around $z/H = 0.1$ for $t > 3$ h.

In Fig. 10, a negative heat flux is observed near the top region of the tank height, which indicates energy transfer from the water in the TST to the brine in the spiral path. Note that this result is related to the inlet position of the spiral flow path. As shown in Fig. 2, the spiral jacket almost completely covered the cylindrical tank, and

the inlet of the brine flow path was located near $z/H = 0.8$. Thus, the negative heat flux observed at the top of the TST was caused by stagnant brine in those regions. However, the magnitude of the negative heat flux is relatively small and decreases as the brine flow rate increases.

The detailed heat transfer characteristics of natural convection inside the TST are investigated in Fig. 11, where the temperature and velocity boundary layers at the mid-height ($z/H = 0.5$) and at $t = 2.5$ h are presented. In Fig. 11, the boundary layer thickness is estimated to be about 0.4 cm for the temperature distribution and about 0.8 cm for the vertical velocity distribution. Fig. 11 clearly shows that a higher brine flow rate increases the intensity of natural convection inside of the spiral-jacketed TST. A higher temperature gradient near the tank wall and a larger magnitude of vertical velocity are caused by an increase in the brine flow rate. This result can be readily explained by referring to the heat flux distribution shown in Fig. 10. At the brine flow rate higher than 8 ℓ/min, energy transfer from the brine to the water is more active in the lower-half region of the TST, and this increases the natural convection intensity compared to situations with uniform energy transfer. However, at a brine flow rate lower than 2 ℓ/min, energy transfer is more active in the upper-half region of the TST, which reduces the intensity of natural convection.

Fig. 11(b) shows that the vertical velocity in the boundary layer near the heated tank wall is positive, but the velocity in the remaining circular plane of the TST is negative. This result indicates

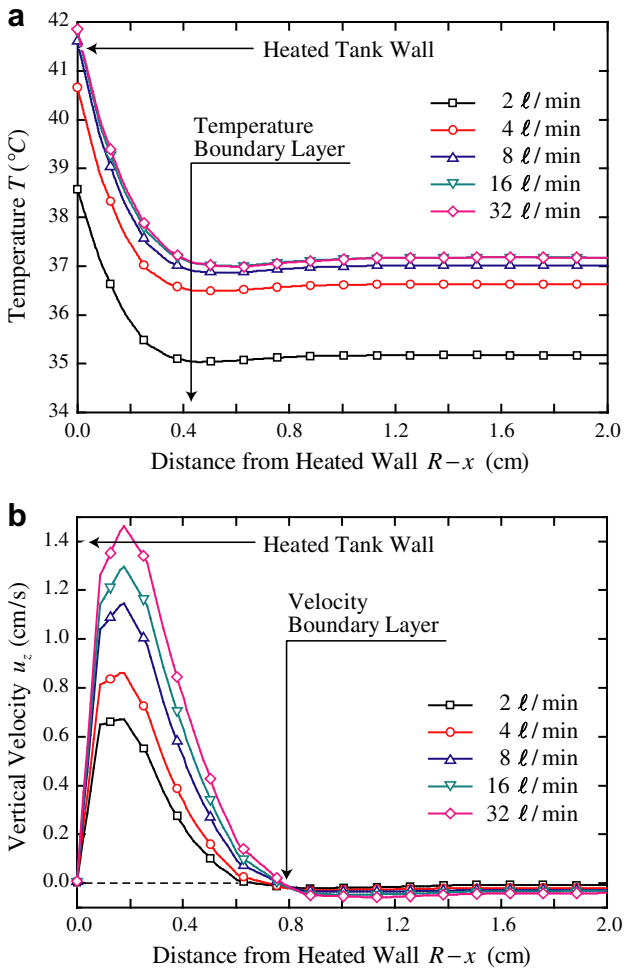

Fig. 11. Natural convection near the heated wall of the spiral-jacketed TST at $z/H = 0.5$ and $t = 2.5$ h: (a) temperature distribution and (b) vertical velocity distribution.

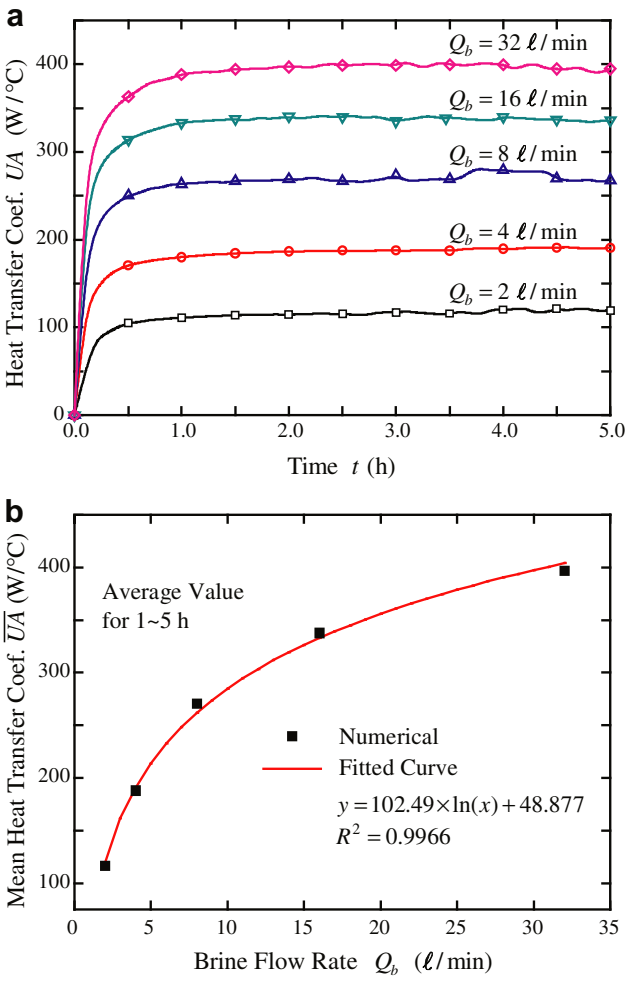

Fig. 12. Overall heat transfer coefficient for the spiral-jacketed TST: (a) temporal history and (b) mean coefficient.

that the natural convection generates a global circulating motion of the water in the TST, characterized by a fast upward flow through the thin annular boundary layer near the heated tank wall and a slow downward flow through a large circular area at the core of the TST. Thus, it is possible to estimate the circulation time, t_{circ}, that is required to completely circulate water in the TST through the boundary layer. To determine t_{circ}, the volumetric water flow rate through the boundary layer was calculated first by integrating the vertical velocity profile shown in Fig. 11(b), and then the tank volume, V_t, was divided by the volumetric flow rate. The estimated circulation time, t_{circ}, is summarized in Table 3. According to Table 3, circulation of the total volume of water in the TST occurs about once per hour for $Q_b = 32$ ℓ/min, whereas a complete circulation requires more than 2.5 h for $Q_b = 2$ ℓ/min. Note that thermal stratification can be more easily disturbed by using a higher brine flow rate, as there is more intense circulation of liquid water inside the TST.

Finally, the overall heat transfer coefficient of the spiral-jacketed TST is shown in Fig. 12. The overall heat exchange coefficient, UA, was calculated as

$$\rho_w c_{pw} V_t \frac{\partial T_{w,\mathrm{mix}}}{\partial t} = UA(T_{s,\mathrm{in}} - T_{w,\mathrm{mix}}). \quad (15)$$

Note that the inlet temperature at the spiral flow path is used in the definition of UA. Fig. 12(a) shows that the overall heat transfer coefficient rapidly increases during the first 1 h period, and then

remains relatively constant. Thus, the average heat transfer coefficient, $\overline{UA}$, was calculated by averaging UA from 1 h to 5 h. Fig. 12(b) shows that a higher brine flow rate results in a higher overall heat transfer coefficient, which indicates that better heat transfer characteristics can be obtained by increasing the brine flow rate. One reason for the better heat transfer properties with a higher Q_b is the enhanced natural convective heat transfer inside the TST, as confirmed by Fig. 11. Another reason may be the enhanced forced convection heat transfer in the spiral brine path due to more active secondary flow at a higher Q_b.

4. Conclusion

Using a validated CFD model, this study numerically investigated the effect of the brine flow rate on the performance of a spiral-jacketed TST installed in an SDHW system. For realistic simulation of the 5-h charging process, experimental solar radiation and ambient temperature data that were measured during operation of the SDHW demonstration system were incorporated into the CFD model. The thermal performance of the spiral-jacketed TST was evaluated on the basis of the energy and exergy analyses. In addition, the thermal stratification and the heat transfer characteristics in the spiral-jacketed TST were also investigated in detail.

The numerical results showed that a higher brine flow rate generally enhanced the thermal efficiency of the TST, but the enhancement became less noticeable as the brine flow rate increased. The exergy of the TST was found to exhibit a maximum value at the brine flow rate of about 4 ℓ/min among the simulated flow rates. From this result, the optimum flow rate for the brine circulation was estimated to be about 2–8 ℓ/min. The results also showed that higher thermal stratification in the TST can be achieved by using a smaller brine flow rate. This trend was explained based on the observed transition in the heat flux distribution at the tank wall with respect to the brine flow rate. The transition in the heat flux distribution was also found to affect the natural convection inside the TST, which influenced the degree of thermal stratification.

Acknowledgement

This work was supported by the second stage of Brain Korea 21 (BK21) Project in 2010.

References

[1] J.A. Duffie, W.A. Beckman, Solar Engineering of Thermal Processes, second ed. John Wiley & Sons, New York, 1991.
[2] D.Y. Goswami, J.F. Kreider, Principles of Solar Engineering, second ed. CRC Press, New York, 2000.
[3] R.B. Farrington, C.E. Bingham, Testing and Analysis of Load-side Immersed Heat Exchangers for Solar Domestic Hot Water Systems. Solar Energy Research Institute Technical Report, 1987.
[4] M.G. Parent, T.H. Van der Meer, K.G.T. Hollands, Natural convection heat exchangers in solar water heating systems: theory and experiment, Solar Energy 45 (1990) 43–52.
[5] S.D. Dahl, J.H. Davidson, Performance and modeling of thermosyphon heat exchangers for solar water heaters, Journal of Solar Energy Engineering 119 (1997) 193–200.
[6] R.K. Shah, D.P. Sekulic, Fundamentals of Heat Exchanger Design. John Wiley & Sons, New York, 2003.
[7] L.J. Shah, S. Furbo, Correlation of experimental and theoretical heat transfer in mantle tanks used in low flow SDHW systems, Solar Energy 64 (1998) 245–256.
[8] L.J. Shah, G.L. Morrison, M. Behnia, Characteristics of vertical mantle heat exchangers for solar water heaters, Solar Energy 67 (1999) 79–91.
[9] L.J. Shah, Heat transfer correlations for vertical mantle heat exchangers, Solar Energy 69 (2001) 157–171.
[10] S. Knudsen, S. Furbo, Thermal stratification in vertical mantle heat-exchangers with application to solar domestic hot-water systems, Applied Energy 78 (2004) 257–272.
[11] S. Knudsen, G.L. Morrison, M. Behnia, S. Furbo, Analysis of the flow structure and heat transfer in a vertical mantle heat exchanger, Solar Energy 78 (2005) 281–289.
[12] N. Altuntop, Z. Kilik, V. Ozceyhan, O. Kincay, Effect of water inlet velocity on thermal stratification in a mantled hot water storage tank, International Journal of Energy Research 30 (2006) 163–176.
[13] S. Furbo, S. Knudsen, Improved design of mantle tanks for small low flow SDHW systems, International Journal of Energy Research 30 (2006) 955–965.
[14] L. Kenjo, C. Inard, D. Caccavelli, Experimental and numerical study of thermal stratification in a mantle tank of a solar domestic hot water system, Applied Thermal Engineering 27 (2007) 1986–1995.
[15] Y.C. Soo Too, G.L. Morrison, M. Behnia, Performance of solar water heaters with narrow mantle heat exchangers, Solar Energy 83 (2009) 350–362.
[16] L.H. Gunnewiek, S. Nguyen, M.A. Rosen, Evaluation of the optimum discharge period for closed thermal energy storages using energy and exergy analyses, Solar Energy 51 (1993) 39–43.
[17] M.A. Rosen, The exergy of stratified thermal energy storages, Solar Energy 71 (2001) 173–185.
[18] M.A. Rosen, I. Dincer, Exergy methods for assessing and comparing thermal storage systems, International Journal of Energy Research 27 (2003) 415–430.
[19] D. Reindl, S.K. Kim, Y.T. Kang, H. Hong, Experimental verification of a solar hot water heating system with a spiral-jacketed storage tank, Journal of Mechanical Science and Technology 22 (2008) 2228–2235.
[20] J.H. Nam, M.C. Kim, C.J. Kim, H. Hong, CFD analysis for spiral-Jacketed thermal storage tank in solar heating systems, Korean Journal of Air-Conditioning and Refrigeration Engineering 20 (2008) 645–653.
[21] Z. Qureshi, B. Gebhart, Transition and transport in buoyancy driven flow in water adjacent to a vertical uniform flux surface, International Journal of Heat and Mass Transfer 21 (1978) 1467–1478.
[22] E. Papanicolaou, V. Belessiotis, Transient natural convection in a cylindrical enclosure at high Rayleigh numbers, International Journal of Heat and Mass Transfer 45 (2002) 1425–1444.
[23] Y.H. Han, R.Z. Wang, Y.J. Dai, Thermal stratification within the water tank, Renewable and Sustainable Energy Reviews 13 (2009) 1014–1026.
[24] M.S. Shin, H.S. Kim, D.S. Jang, S.N. Lee, Y.S. Lee, H.G. Yoon, Numerical and experimental study on the design of a stratified thermal storage system, Applied Thermal Engineering 24 (2004) 17–27.
[25] L.J. Shah, E. Andersen, S. Furbo, Theoretical and experimental investigations of inlet stratifiers for solar storage tanks, Applied Thermal Engineering 25 (2005) 2086–2099.
[26] N. Altuntop, M. Arslan, V. Ozceyhan, M. Kanoglu, Effect of obstacles on thermal stratification in hot water storage tanks, Applied Thermal Engineering 25 (2005) 2285–2298.

Glossary

A: area, m^2
c_p: specific heat, J kg^{-1} K^{-1}
E: energy, J
F_R: collector heat removal factor
G_t: solar radiation intensity, W m^{-2}
g_j: gravitational acceleration component, m s^{-2}
k: thermal conductivity, W m^{-1} K^{-1}
P_p: pump power, W
p: pressure, Pa
q: heat flux at tank wall, W m^{-2}
Q_b: volume flow rate of brine, m^3 s^{-1}
t: time, s
T: temperature, K
u_j: velocity component, m s^{-1}
U_L: overall heat loss coefficient, W m^{-2} K^{-1}
UA: overall heat transfer coefficient, W K^{-1}
V: volume, m^3

Greek letters
β: volume expansion coefficient, K^{-1}
ΔT_w: top/bottom temperature difference, K
η: thermal efficiency
μ: dynamic viscosity, Pa s
ρ: density, kg m^{-3}
$\tau\alpha$: transmittance-absorptance product
Ξ: exergy, J

Subscripts and superscripts
0: initial or reference condition
a: ambient
b/w: brine/water
cen: centerline
c/s/t: collector/spiral path/tank
in/out: inlet/outlet
old: previous time step